The Multi-center Airborne Coherent Atmospheric Wind Sensor

Jeffry Rothermel,[*] Dean R. Cutten,[+] R. Michael Hardesty,[#] Robert T. Menzies,[@]
James N. Howell,[#] Steven C. Johnson,[&] David M. Tratt,[@]
Lisa D. Olivier,[#] and Robert M. Banta[#]

ABSTRACT

In 1992 the atmospheric lidar remote sensing groups of the National Aeronautics and Space Administration Marshall Space Flight Center, the National Oceanic and Atmospheric Administration/Environmental Technology Laboratory (NOAA/ETL), and the Jet Propulsion Laboratory began a joint collaboration to develop an airborne high-energy Doppler laser radar (lidar) system for atmospheric research and satellite validation and simulation studies. The result is the Multi-center Airborne Coherent Atmospheric Wind Sensor (MACAWS), which has the capability to remotely sense the distribution of wind and absolute aerosol backscatter in three-dimensional volumes in the troposphere and lower stratosphere.

A factor critical to the programmatic feasibility and technical success of this collaboration has been the utilization of existing components and expertise that were developed for previous atmospheric research by the respective institutions. For example, the laser transmitter is that of the mobile ground-based Doppler lidar system developed and used in atmospheric research for more than a decade at NOAA/ETL.

The motivation for MACAWS is threefold: 1) to obtain fundamental measurements of subsynoptic-scale processes and features to improve subgrid-scale parameterizations in large-scale models, 2) to obtain datasets in order to improve the understanding of and predictive capabilities for meteorological systems on subsynoptic scales, and 3) to validate (simulate) the performance of existing (planned) satellite-borne sensors.

Initial flight tests were made in September 1995; subsequent flights were made in June 1996 following system improvements. This paper describes the MACAWS instrument, principles of operation, examples of measurements over the eastern Pacific Ocean and western United States, and future applications.

1. Introduction

Being able to remotely measure the wind over a three-dimensional volume has been the stuff of meteorologists' dreams for many decades. This dream has led to ground-based dual-Doppler radar and airborne pseudo-dual-Doppler radar such as the Electra Doppler Radar (ELDORA; Wakimoto et al. 1996), which provide high-resolution wind measurements in volumes with cloud and precipitation. An obvious question is, what about the majority of the atmosphere that lies outside of cloud? A new system, an airborne Doppler lidar, provides exactly this kind of measurement: gridded volumes of the horizontal winds outside of clouds. Scattering targets for this remote sensing instrument are naturally occurring aerosols, which are present in sufficient concentrations, particularly in the lowest 3–4 km of the troposphere, to obtain Doppler winds (e.g., Rothermel et al. 1989). This new system, called the Multi-center Airborne Coherent Atmospheric Wind Sensor (MACAWS), represents a collaboration among the atmospheric lidar remote sensing groups of the National Aeronautics and Space Administration/Marshall Space Flight Center (NASA/MSFC), the Jet Propulsion Laboratory (JPL), and the

[*]Global Hydrology and Climate Center, NASA/George C. Marshall Space Flight Center, Huntsville, Alabama.
[+]University of Alabama in Huntsville, Huntsville, Alabama.
[#]NOAA/Environmental Technology Laboratory, Boulder, Colorado.
[@]Jet Propulsion Laboratory, Pasadena, California.
[&]NASA/George C. Marshall Space Flight Center, Huntsville, Alabama.
Corresponding author address: Dr. Jeffry Rothermel, Global Hydrology and Climate Center, 977 Explorer Boulevard, Huntsville, AL 35806.
E-mail: jeffry.rothermel@msfc.nasa.gov
In final form 11 December 1997.

Atmospheric Lidar Division of the Environmental Technology Laboratory (ETL) of the National Oceanic and Atmospheric Administration (NOAA) Environmental Research Laboratories. It represents a blending of technologies, highlighted by the use of the NOAA/ETL mobile Doppler lidar, previously employed for more than a decade in the ground-based mode, being installed on the NASA DC-8 research aircraft in a side-looking configuration. This system has the potential to significantly enhance our understanding of a wide variety of atmospheric phenomena.

a. History of measurement concept

The concept of wind field measurement with airborne Doppler laser radar, or lidar, was inspired by the need for better observations in nonprecipitating regions surrounding severe storms (Bilbro and Vaughan 1978). It was argued that such observations could improve our understanding of the evolution and dynamics of extreme weather events, including tornadic thunderstorms, severe turbulence, and hurricanes. Moreover, the scientific utility of lidar measurements could be enhanced through coordination with conventional, ground-based sensors, especially Doppler radar.

The measurement concept became a reality in 1981 with the first flights of a low-energy (14 mJ pulse^{-1}) Doppler lidar system that was originally developed for studies of clear-air turbulence (Jelalian et al. 1972; Bilbro et al. 1984). The lidar system was configured to obtain wind measurements within a horizontal plane relative to the aircraft using a pseudo-dual-Doppler technique. In view of lidar measurement capabilities in clear air, research objectives were expanded to include studies of nonsevere flows as well. Demonstration measurements included flow over complex terrain (Cliff et al. 1985), planetary boundary layer structure (Eilts et al. 1984; Eilts et al. 1985), and thunderstorm outflows (Emmitt 1985; Bluestein et al. 1986; McCaul et al. 1986, 1987). With the soundness of the airborne Doppler lidar wind measurement concept thus confirmed, enhancements were made to enable wind field measurements at multiple vertical levels, as well as to improve velocity accuracy in the presence of turbulence (Bilbro et al. 1986). Subsequent flights were made in 1984, and studies included lee mountain waves (Blumen and Hart 1988) and the extended sea breeze (Carroll 1989).

b. Scientific motivation

In the 1980s a number of significant developments occurred that would contribute to the development of an airborne Doppler lidar with improved research capabilities. First, technological advances continued to yield higher-energy, frequency-stable CO_2 laser transmitters (Batten et al. 1987; Theon et al. 1991). The significance of this is that measurement coverage, and hence the scientific utility, is roughly proportional to the transmitted energy per pulse. An example of technological advancement during that time period is the upgraded laser transmitter used within a mobile, ground-based Doppler lidar system that was developed by NOAA/ETL (Post and Cupp 1990). The development of this type of transmitter began in 1978 at JPL (Megie and Menzies 1979). The previous laser transmitter (0.1 J pulse^{-1}) enabled horizontal coverage of measured velocities out to only ~6–15 km, whereas the upgraded lidar system (up to ~1 J pulse^{-1}) is now capable of coverage to 10–30 km subject to sufficiency of aerosols and other atmospheric conditions. As a ground-based system, the NOAA/ETL Doppler lidar has been deployed successfully in a variety of locations. The analyses of simultaneous aerosol backscatter and velocity measurements were particularly useful for determining the role of winds in the transport of aerosols into and out of a valley near Vancouver, British Columbia, Canada (Banta et al. 1997). Other studies using simultaneous velocity and backscatter data include measurements of the horizontal wavelength of trapped lee waves (Ralph et al. 1997) and the investigation of the structure of a prescribed forest fire (Banta et al. 1992). Further examples of the lidar's versatility include detailed measurements of mesoscale features. Such studies include measurements of a well-defined canyon outflow that was narrow enough to escape detection by an enhanced network of sensors, yet strong enough to affect dispersion of pollutants (Banta et al. 1995) and the evolution and vertical structure of the Monterey Bay, California, sea breeze (Banta et al. 1993). As demonstrated in Clark et al. (1994), a comparison of windstorm model simulations to lidar measurements of the same event shows that the high spatial resolution of lidar data make the data useful for model validation. By combining lidar backscatter measurements with those of a Ka-band radar, Intrieri et al. (1993) have shown that information about cirrus cloud particle sizes can be retrieved.

A second significant development was the emergence of a heightened awareness of climate and global change, accompanied by stronger scientific and programmatic emphasis on observing, describing, and predicting geophysical processes on a wide range of

spatial and temporal scales. An example is the U.S. Global Change Research Program, a component of which is the NASA Earth Science Enterprise. Knowledge of the global wind field is widely recognized as being fundamental to advancing the understanding and prediction of climate, the hydrological cycle, and weather (Baker et al. 1995).

Finally, beginning in the 1970s a number of independent design and performance simulation studies supported the feasibility of satellite-borne, lidar-based Doppler wind sensors using current technology (e.g., Huffaker et al. 1984; Menzies 1986; NASA 1982, 1987). In the absence of a measurement heritage for satellite Doppler wind lidar (SDWL), simulations with airborne Doppler lidar offer the opportunity to reduce uncertainties in lidar simulation models and to begin the development of interpretive skills. More recently, it is noted that the U.S. Weather Research Program has so far identified a number of research issues to which airborne Doppler wind lidar measurements are ideally and uniquely suited (Emanuel et al. 1995).

c. Program implementation

In response to these factors, NASA and NOAA initiated a research program in April 1992 to develop an airborne Doppler wind lidar with improved scientific utility compared to previous systems. The scientific motivation has been threefold: 1) to obtain fundamental measurements of subsynoptic-scale processes and features that may be used to improve model parameterizations in large-scale models; 2) to obtain datasets to improve understanding and predictive capabilities of meteorological systems on subsynoptic scales, that is, less than 300 km; and 3) to simulate the performance of prospective satellite Doppler lidars for global tropospheric wind measurement. More recently the need has arisen to validate planned satellite wind sensors, such as a proposed small-satellite Doppler wind lidar, as well as existing sensors that are based on other measurement techniques.

Although NASA/MSFC, NOAA/ETL, and JPL have been primarily responsible for the MACAWS development and operation, additional involvement has come from universities and private industry. Flight planning and data analysis are accomplished both within this team and through collaborations with external investigators.

A factor critical to the programmatic feasibility and technical success of this program has been the use of components and expertise that were developed in the course of previous airborne and ground-based atmospheric research by our respective institutions.[1] The laser transmitter for MACAWS is borrowed from the mobile ground-based lidar system developed by NOAA/ETL (Post and Cupp 1990), which was upgraded with a more powerful laser transmitter before undergoing additional modifications to achieve flightworthiness. The optical table used to support the laser and other optical components, which by design must help to preserve the optical alignment under a variety of flight conditions, was developed in part for a program to survey the global aerosol backscatter distribution (Menzies and Tratt 1994). The telescope and other components (described later) were developed for NASA/MSFC atmospheric research programs (Bilbro et al. 1984; Bilbro et al. 1986). Some hardware modifications were required to ensure flight safety, operational reliability, and compatibility with the aircraft environment. Laboratory integration and ground tests were conducted at JPL, Pasadena, California, during 1 March–19 July 1995; the first atmospheric returns were obtained on 18 May 1995. The first flight tests were conducted in September 1995; subsequent flight experiments were conducted in June–July 1996. In the intervening time between flight programs, repairs and modifications were performed in order to improve performance, especially under turbulent flow conditions.

This article provides an overview of the MACAWS instrument and measurement capabilities (section 2), measurement uncertainties (section 3), a summary of our two previous flight experiments including sample results (section 4), an abbreviated set of research objectives that we plan to address in future missions (section 5), and some conclusions based on our experience with the development and flight of what is the most powerful and sophisticated airborne coherent Doppler lidar to date (section 6).[2]

2. MACAWS description

This section describes the principal subsystems, functions, and atmospheric sampling methods. The

[1]We estimate that at least $4,000,000 has been saved by using our existing lidar equipment and expertise compared to the cost of designing, fabricating, field testing, and debugging a new lidar system with comparable measurement capabilities.

[2]A Web site has been created at http://www.ghcc.msfc.nasa.gov/macaws.html. More complete technical details may be found there, along with additional examples of measurements from previous flights.

principal differences between MACAWS and the system described by Bilbro et al. (1986) are threefold. First and foremost, the injection-seeded, transverse-excited atmospheric pressure (TEA) laser transmitter from the NOAA/ETL windvan has been used (Post and Cupp 1990), which provides a factor of over 50 improvement in pulse energy compared to the system flown in 1981 and 1984. Second, the optical elements in the scanner have been modified to permit measurements over a greater angular range as described below. Finally, the flight computer system provides more extensive, real-time data processing with improved data and instrument status displays, in a much smaller volume and mass unit.

A more detailed technical description and performance assessment of the system are given by Howell et al. (1996). Although other airborne coherent Doppler lidars have been developed (Targ et al. 1996; Richmond and Jewell 1997), or are being developed (Werner 1989), to our knowledge MACAWS is the only system specifically designed to measure high-resolution fields of two-dimensional wind velocities over a three-dimensional volume.

a. Instrument description

MACAWS consists of the following major subsystems: laser transmitter, receiver, telescope, optical table, scanner, inertial measurement unit, and computer. Table 1 summarizes the principal instrument and performance characteristics. The transmitter is a frequency-stable, TEA CO_2 laser (Post and Cupp 1990). The receiver consists of a cryogenically cooled infrared detector and supporting optics and electronics configured for coherent signal detection (Post and Cupp 1990; Menzies and Tratt 1994). The folded telescope consists of a 0.3-m diameter off-axis paraboloidal primary mirror and secondary mirror shared by the transmitter and receiver in a monostatic configuration. The table assembly consists of a ruggedized optical table, separable into two sections to facilitate integration; the table itself is upheld by a three-point support structure that is fastened to the aircraft seat tracks. The scanner is composed of two computer-controlled, independently rotating germanium wedges that refract the transmitted beam in the desired direction (Amirault and DiMarzio 1985). The original scanner had the capability to refract the beam anywhere within a full cone angle of ~40°. In the present configuration the wedges have been replaced with elements of greater angular thickness that permit scanning anywhere within a full cone angle of ~64°. A dedicated inertial measurement unit (IMU), mounted beneath the scanner, senses aircraft attitude and speed parameters; the IMU is interrogated at 20 s^{-1} (Bilbro et al. 1986). This information is required to derive ground-relative wind motion by a process described later. The computer consists primarily of a UNIX-based "operations con-

TABLE 1. MACAWS characteristics.

Characteristic	Nominal	Range
Wavelength (μm)	10.6	9–11
Transmitter	TEA CO_2 gas laser	
Energy per pulse (J, long pulse mode)	0.8	0.6–1.0
Beamwidth to e^{-2} power points	20 cm	
Pulse duration (μs)	3	0.4, 3[a]
Laser linewidth (kHz)	~300	
Pulse repetition frequency PRF (s^{-1})	20	0.1–30
Telescope diameter (m)	0.3	
Line-of-sight resolution (m)	300	150–1200
Number of scan planes	5	1–5
Vertical resolution (km)[b]		0–12.5
Wind velocity accuracy (m s^{-1})	~1	
Nyquist radial velocity (m s^{-1})[c]	75	
Coverage (km)[d]		10–30

[a]Duration in which 80% of the pulse energy is emitted.
[b]Dependent on range and angular separation between scan planes.
[c]Actual ground-relative velocity limits may differ depending on relationship between line-of-sight components of air speed and ground velocity.
[d]Dependent on distribution of aerosol backscatter and extinction.

trol system" (OCS) that orchestrates the functioning of each subsystem. The OCS also processes, displays, and stores raw lidar data (in limited quantities) and processed data, along with scanner settings, IMU data, and aircraft housekeeping data. MACAWS is presently configured for the NASA DC-8 research aircraft, which has a service ceiling of 12.5 km and a range of over 9400 km (NASA 1994).

Laser pulses are transmitted to the atmosphere through the scanner, which is mounted within the left side of the aircraft ahead of the wing. Upon exiting the aircraft the beam is eyesafe for any combination of laser-operating parameters, owing to the range of middle infrared wavelengths determined by the choice of a CO_2 laser and to expansion of the laser beam by the telescope (American National Standards Institute 1993). Aerosols, clouds, or the earth's surface scatter a small portion of the incident radiation backward along the line of sight (LOS) to the receiver. In order to maintain precise beam pointing, IMU measurements are received by the OCS, which issues commands to the receiver and scanner to compensate for aircraft attitude and speed changes at 20 s^{-1} similar to the IMU interrogation rate. Using the same IMU measurements during signal processing, the OCS and receiver calculate and subtract the frequency contribution to the Doppler-shifted signal representing the component of aircraft motion along the line of sight; details of the signal processing are summarized later. The resulting range-resolved LOS velocities represent the components of wind motion with respect to earth coordinates. Measurement coverage varies with lidar system settings (laser output energy, pulse repetition frequency, LOS resolution, and number of pulses averaged) and atmospheric conditions (aerosol backscatter distribution and attenuation by water vapor, carbon dioxide, and clouds). Onboard displays of LOS velocity, two-dimensional wind fields, and backscattered signal intensity provide in-flight mission guidance as well as enabling real-time assessment of subsystem performance and overall data quality. For additional guidance, visible and infrared imagery from polar-orbiting satellites are available from a satellite weather facsimile receiver (NASA 1994).

As implied by the name of the instrument, MACAWS uses coherent detection of the backscattered radiation (Menzies and Hardesty 1989), meaning that the phase front of the return signal is matched to that of a stable-frequency reference optical beam (the so-called local oscillator laser) before the two signals undergo mixing at the signal detector. The reference frequency is offset from that of the nominal transmitter frequency, so that the detector registers a time-varying beat signature, the resolved frequency of which expresses the frequency difference between the emitted and Doppler-shifted return radiation. Atmospheric signal processing is done in real time; a poly-pulse-pair velocity estimation algorithm, implemented digitally as a matched-filter frequency domain estimator (Rye and Hardesty 1994), is used to calculate LOS velocities (Lee and Lee 1980). For each range gate, the fast Fourier transform of the truncated autocorrelation function is calculated from digitized, complex samples of the time-varying output of the signal detector. The peak of the frequency spectrum is then found with high resolution by fitting a quadratic curve to the three points nearest the peak of the FFT. The peak of the fitted function corresponds to the LOS velocity estimate. Pulses with excessive frequency variation due to system anomalies, such as transient optical misalignments due to turbulence, are flagged and excluded from signal processing and are termed "bad" pulses. During signal processing the LOS resolution may be varied from 0.15 to 1.2 km, although in practice the resolution is usually varied over 0.15–0.3 km. The minimum range at which a signal can be detected is 1.0–1.5 km for 3-μs pulse duration (containing 80% of pulse energy), owing to the presence of a weak pulse "tail" that causes optical and radio frequency interference at close range.

b. Calibration

Before research flights commence, the IMU, scanner, and lidar transceiver are each calibrated in the following sequence. First, the IMU is physically aligned with the aircraft so that measurements of roll, pitch, and pointing direction agree with those of the DC-8 inertial navigation system (INS). Second, scanner pointing is calibrated relative to the IMU-indicated aircraft orientation (Amirault and DiMarzio 1985). This procedure involves directing the lidar beam in stages out to a succession of surveyed reference points located up to 300 m from the aircraft. The set of recorded wedge positions, corresponding to the survey points, is used to derive a set of scanner alignment parameters. Finally, the intensity response of the lidar transmitter–receiver is calibrated by comparing backscattered signals from a target of known reflectance with expected signal intensity calculated from the lidar signal-to-noise (SNR) equation using measured system parameters (Post and Cupp 1990). The resulting calibration factor permits conversion of rela-

tive signal intensity (dB) to units of absolute backscatter (m^{-1} sr^{-1}).

c. Sampling methods

The manner in which the atmosphere is sampled with the lidar beam depends critically on the science objective(s), three-dimensional distribution of the feature or process of interest, aircraft altitude, aerosol backscatter distribution, attenuation, and range to target. Figures 1a–c illustrate sampling geometries that are now described in order of increasing complexity; examples of measurements are given in section 4.

1) VERTICAL PROFILING

The beam can be refracted up to 32° upward or downward relative to the aircraft. Two modes of vertical profiling are possible. Figure 1a illustrates the case of downward pointing.

(i) Quasi-vertical cross section

The first vertical profiling mode is accomplished by maintaining a constant flight heading. The resulting distribution of measurements is similar to the familiar vertical cross section, which is subject of course to the presence of horizontally distributed gradients in wind and aerosols. This sampling strategy may be used to measure the quasi-vertical distribution of aerosol backscatter over relatively large horizontal distances with an equivalent vertical resolution of ≤ 75 m.

(ii) Quasi-velocity azimuth display

To achieve this mode of vertical profiling, the aircraft is directed into a turn at constant roll angle. The resulting sampling pattern resembles a velocity azimuth display common to ground-based radar. Two principal applications are possible. First, a single horizontal wind profile above or below the aircraft may be obtained by techniques that were originally developed for ground-based radar, for example, Lhermitte and Atlas (1961) and Browning and Wexler (1968). Second, by altering the roll angle between orbits, the angular dependence of the surface scattering may be observed. For roll angles greater than ~40° (equivalent to nadir angles less than 20°), the resulting g-force on the optical table causes optical misalignment and loss of signal for which the built-in, autonomously operated alignment devices cannot compensate.

2) TWO-DIMENSIONAL SCANNING

A unique feature of MACAWS is the capability to remotely sense two-dimensional (2D) wind fields in clear air. The sampling method, a pseudo-dual-Doppler technique referred to as coplanar scanning, was demonstrated in 1981 with airborne coherent Doppler lidar (Bilbro et al. 1984). Details of the signal processing and wind estimation methodology are described by McCaul et al. (1986). Figure 1b illustrates a plan view of the sampling pattern of lidar beams. Each beam may be composed of three or more pulses that are combined during signal processing to improve LOS velocity accuracy and coverage (Lee and Lee 1980). While scanning the beam is alternately directed ~20° forward and aft of normal relative to the

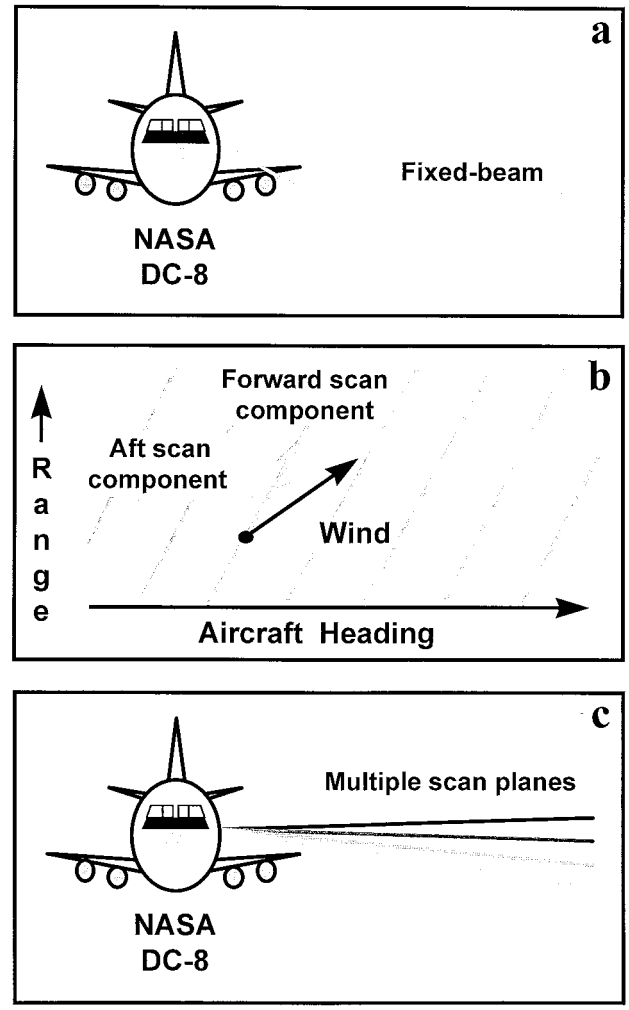

FIG. 1. MACAWS sampling capabilities. (a) Lidar beam orientation is fixed for quasi-vertical profiles of line-of-sight velocity and aerosol backscatter, or for studies of angular scattering dependence, over a vertical range of ±32°. (b) Coplanar scanning is performed to measure a single wind field, with 40° in-plane angular separation between forward and aft scans. (c) Coplanar scanning is performed at up to five elevation angles at arbitrary angular spacing to achieve volumetric coverage, over a vertical range ±25°.

aircraft heading. At each "point" of intersection, a 2D velocity can be calculated due to the angular separation between perspectives. This estimate represents the component of wind motion within the scan plane. Without compensation for aircraft motions (described above), turbulence experienced by the aircraft could cause the scanner to misdirect one or more beams outside of the scan plane. The OCS uses IMU measurements of aircraft pitch, roll, and track angle, to compensate by issuing appropriate commands to the scanner. Minimum response time of the scanner (~100 ms or less) is influenced by the inertia of the wedges (each with a mass of 9.5 kg) and the position to which the scanner must slew. The angular thickness of the wedges (~5.0°) limits the vertical angular limits of the 2D measurement capability to ±25°, beyond which there is insufficient angular separation between fore and aft beams to calculate 2D velocity accurately.

3) Three-dimensional scanning

The 2D scanning technique may be used to achieve three-dimensional (3D) coverage by generating multiple scan planes (Fig. 1c), a concept that was demonstrated successfully in 1984 (Bilbro et al. 1986). The present OCS capability permits up to five scan planes, with arbitrary vertical angular spacing depending on the research objective. In general the vertical extent of the domain over which measurable signals may be obtained is a function of 1) aircraft altitude, which is subject to air traffic control restrictions and aircraft service ceiling; 2) angular separation between uppermost and lowermost scan planes, which is subject to the refractive limit of the scanner; 3) aerosol backscatter distribution, which is a function of the aerosol physical, chemical, and optical properties; and 4) attenuation of the incident and scattered laser radiation, which depends on concentrations of water vapor, CO_2, aerosols, and the optical thickness of cloud (if present).

Resolution along the flight track Δx in each scan plane may be expressed by the following approximation for both 2D and 3D scanning:

$$\Delta x \cong \left[2(n_a - 1)d_1 + 2n_a\left(\frac{n_g + n_b}{P}\right) + 2d_2 \right] V_g, \quad (1)$$

where d_1 is the delay in repositioning the scanner wedges to an adjacent elevation angle in the fore or aft direction (~0.1 s), d_2 is the scanner delay between the fore and aft pointing directions (~0.6 s), n_a is the number of scan planes, n_g is the number of pulses averaged during signal processing, n_b is the number of pulses rejected during signal processing, P is the laser pulse repetition frequency (s^{-1}), and V_g is the aircraft ground speed. Turbulence may slightly increase the time required to reposition the scanner wedges. Turbulence can also cause brief periods of laser mode degradation or frequency jitter; the onboard pulse quality discriminator rejects these pulses. Both effects degrade the along-track resolution. For the case of measurements in the planetary boundary layer (PBL) assuming $V_g = 125$ m s^{-1}, $P = 20$ s^{-1}, $n_a = 5$, $n_b = 2$, and $n_g = 10$, $\Delta x \cong 1.0$ km.

d. Comparison with Doppler radar

The primary advantage to Doppler lidar is the capability to measure the wind in optically clear air; thus airborne lidar can complement airborne radar in measurement scenarios containing optically thick clouds and precipitation. Hydrometeors constitute the primary source of scattering targets for radar, whereas coherent Doppler lidar can utilize backscatter from aerosol particles (of order 1 μm in diameter), clouds, and, to a lesser extent, small hydrometeors. Propagation within optically thick cloud is limited by extinction due to scattering and absorption by the cloud particles. However, attenuation by thin or subvisual cirrus can be quite small, especially if probed from nonoblique angles. The ground-based NOAA/ETL lidar has been used to study microphysics and dynamics in cirrus clouds, often penetrating to depths of 3–4 km for optically thin clouds (Intrieri et al. 1995). For low concentrations of ice crystals, therefore, coverage may even be enhanced by clouds. Laser radiation in the middle infrared is absorbed by water vapor, which can diminish sensitivity at extended ranges in moist boundary layers.

Whereas Doppler returns from aerosols are generally representative of the mean wind, radar returns in optically clear air may exhibit biases. Depending on wavelength, radar returns in the optically clear PBL may be weighted toward refractive index fluctuations associated with inversions or the edges of convective structures (Hardy and Ottersten 1969), insects (during nonwinter seasons), and, to a lesser extent, birds (Eastwood 1967). Insects, which are often a source of radar scatterers in warm-season boundary layers, may be concentrated along convergence lines (Wilson et al. 1980), and certain species may have substantial speeds relative to the wind (Fowler and LaGrone 1969). Ra-

dar beam divergence is typically 2–3 orders of magnitude larger relative to coherent lidar. Therefore under marginal radar reflectivity conditions and at low elevation angles, ground clutter contamination can occur, which may bias the velocity estimates, especially over complex terrain (e.g., see Fig. 6, Rothermel et al. 1985). Taking all of these factors into account, nonuniformly distributed targets and their possible independent motions may produce average velocity retrievals that are not entirely representative of small-scale motions in optically clear air. In the optically clear free troposphere, meteorological Doppler radars typically do not obtain returns due to insufficient scatterers. Very high frequency (VHF) wind profilers obtain measurements above the PBL (Weber et al. 1990) owing to refractive index fluctuations; however, the spatial and temporal coverage and resolution are significantly reduced from that of meteorological Doppler radars such as the WSR-88Ds that comprise the National Weather Service network of next-generation Doppler radars (NEXRAD). Because VHF profilers require large antennas, they are not suitable for aircraft deployment.

3. Measurement uncertainties

a. Scanner calibration

For both sets of flights, the uncertainty in scanner pointing was estimated to be ~0.1° root-mean-square (rms) in azimuth and elevation based on least squares analysis of the ground-calibration measurements. For confirmation, observed and expected pointing angles were compared based on aircraft radar altitude and range to surface returns for test flights over sections of the California Central Valley. Angular errors observed in flight were found to be within the rms uncertainty of the ground calibrations. For example, on the checkout flight of 31 May 1996, for an altitude of ~2.13 km above ground level (AGL) and specified scanner elevation angles of −11.5° and −8.0°, actual elevation angles were calculated to be −11.47° and −8.06°, respectively. A 0.1° pointing uncertainty is equivalent to a horizontal or vertical uncertainty of ~17 m at 10-km range, somewhat larger than, but nevertheless consistent with, model predictions based on germanium wedges of slightly smaller angular thickness (Amirault and DiMarzio 1985). In consideration of Eq. (1), the horizontal uncertainty in scattering volume position for an individual pulse is relatively insignificant with respect to the envelope of scattering volumes that comprise an LOS velocity estimate.

b. Velocity

Velocity errors may arise from several sources, consist of random and systematic components, and vary from flight to flight. During scanning, the measured LOS velocity with respect to the aircraft is dominated by aircraft motion. Therefore, it is essential that this large velocity component be characterized accurately in order to determine the residual, ground-relative wind motion. The net effect of random and systematic LOS velocity errors may be quantified when the lidar beam intercepts the land surface, which ideally should exhibit a zero-Doppler shift. Based on analysis of ground hits as well as comparisons at close range with wind measurements derived from the DC-8 INS (NASA 1994), velocity errors of 0.5–4 m s^{-1} may occur with variations from flight to flight owing primarily to periodic errors in the IMU (described below). In this respect, our experiences have been similar to those reported by Carroll (1986), Eilts et al. (1984), and McCaul et al. (1986), the latter two studies having been based on an identical IMU. Carroll (1986) simulated the impact on velocity errors of uncertainties in beam pointing and aircraft speed and the presence of atmospheric wave structure. Velocity measurement errors for the intervening atmosphere may be minimized by correcting for the apparent Doppler velocity of the surface during postprocessing (Rothermel 1987).

1) Beam pointing

Velocity errors arising from scanner calibration uncertainty are relatively small compared to other error sources. For example, an azimuthal pointing error of up to 0.1° at 0° elevation introduces a random velocity error of ≤ 0.4 m s^{-1} for a ground speed of 232 m s^{-1} (450 kt). Lidar operation in the presence of turbulence may introduce additional errors related to scanner performance, described below. The mechanical process by which the alignment of the transmitter laser discharge cavity is maintained introduces additional, random pointing errors ("jitter") of up to 0.02°. At a ground speed of 232 m s^{-1} (450 kt), this effect leads to LOS errors of less than 0.08 m s^{-1}.

2) Inertial measurement unit

For the airborne Doppler lidar system described previously (Bilbro et al. 1984), velocity errors were due principally to undersampling or delayed sampling

of the IMU, from which the update period was ≥ 1 s. For MACAWS, this difficulty has been minimized by interrogating the IMU at the much faster rate of 20 s^{-1}; this improvement was first demonstrated in the modified airborne Doppler lidar described by Bilbro et al. (1986). Although the higher sampling rate effectively reduces systematic errors, random errors may still occur. The reason is that turbulence may introduce aircraft attitude and speed changes, as well as vibrations, at timescales that cannot be resolved by the IMU and that are faster than the positional update rate for the scanner. The resulting pointing error may introduce an additional, but relatively small, LOS velocity component due to aircraft motion (Carroll 1986).

Periodic errors may arise from IMU position measurements due to the Schuler resonance, an inherent source of error in an inertial navigation system (Britting 1971). This error results in an incorrect aircraft ground speed, which is subtracted from the lidar LOS velocities during signal processing. Periodic errors in the MACAWS velocity measurements have been found with amplitude as large as 2–4 m s^{-1}, comparable to findings by Eilts et al. (1984) based on an identical IMU. This periodic error can be quantified by comparison with lower-time-resolution, ground speed measurements derived from the DC-8 global positioning system (GPS) receiver. During postprocessing, GPS-derived ground speeds may be used to recalculate the LOS velocities for cases where IMU-derived ground speeds have significant errors; in this manner an improvement in mean wind velocity errors of 1–4 m s^{-1} can be achieved according to comparisons with DC-8 INS winds. Additional velocity errors occur during aircraft turns; however, these data are not used for calculating two-dimensional wind fields.

3) Lidar transmitter–receiver

When the lidar has been operated in the ground-based mode measuring signals from stationary targets, standard deviations of single-pulse, velocity estimates for the long pulse mode of operation have been found to be 0.6 m s^{-1} (Post and Cupp 1990). The single-shot, short pulse accuracy is degraded to 2.2 m s^{-1} owing to increased signal bandwidth. Airborne measurements of the apparent Doppler velocity of the land surface indicate random errors that cannot be fully accounted for by the factors described in the previous sections. The most likely cause for random velocity errors, apart from the factors cited above, is imprecise characterization of the frequency distribution of the outgoing pulse. A frequency monitor detector is employed in the receiver to sample each outgoing pulse (Post and Cupp 1990). The information obtained by the frequency monitor is used in real time by the signal processor to correct the received signal for variability in the pulse frequency. Analysis of the pulse profile suggests that the duration of the window for the frequency sample may have caused undersampling of the pulse tail. Additional evidence indicates that the frequency monitor detector signal strength occasionally dropped below a level necessary for optimum characterization. A significant effort is currently under way to identify and remedy sources of velocity uncertainty.

4) Signal processing

A digital poly-pulse-pair processor is employed to estimate the first three moments of the frequency distribution of the signal spectrum for each range gate, corresponding to signal power, radial velocity, and velocity variance. This technique is one of several frequency domain, spectral peak estimators that provide good performance at low SNR (Rye and Hardesty 1993). Velocity errors are generally inversely proportional to the square root of the number of lidar pulses integrated (assuming homogeneity over the relevant spatial scales), which during scanning may range from 3 to 20 pulses. The frequency distribution for each transmitted pulse is measured and used by the receiver and OCS to correct the velocity and velocity variance accordingly. For high-SNR signals, velocity uncertainty is on the order of 0.5 m s^{-1}.

c. Aerosol backscatter

Measurement of aerosol backscatter coefficients is carried out by inverting the equation for the coherent lidar signal-to-noise ratio after computing the SNR (e.g., Post and Cupp 1990; Kavaya and Menzies 1985). This estimate requires knowledge of several parameters including system range response, optical efficiency, atmospheric extinction, shot noise level, and pulse energy. For MACAWS, system optical efficiency parameters are measured while the aircraft is stationary; these values are then applied to the flight data. Given an accurate measurement of the system parameters, backscatter coefficients are measurable to within ~3 dB (factor of 2) if the key system parameters do not change significantly between calibrations. By comparison, atmospheric aerosol backscatter at 10.6-μm wavelength may vary over five orders of magnitude or more.

4. Examples of measurements

Following completion of development and ground tests, initial flight tests were conducted over the western United States and eastern Pacific Ocean during 13–26 September 1995. Highest priority was given to the characterization of velocity and scanner pointing accuracy. Subsequently, minor modifications were made to the lidar, receiver, and OCS to improve performance, especially under turbulent conditions (Howell et al. 1996). The system was reflown during 31 May–2 July 1996 over similar areas, as well as over Alaska and Texas in conjunction with other, unrelated experiments. The remainder of this section presents examples of wind and aerosol backscatter measurements.

a. Comparison with aircraft-derived winds

On 31 May 1996 during 1133–1203 UTC, the aircraft flew in a rectangular racetrack pattern at 2.13-km altitude over the San Joaquin Valley of California, southwest of Fresno. The primary objectives of this mission were to verify the scanner calibration and overall system performance. Figure 2 compares lidar winds measured within a 0° scan plane at the closest possible range (1.2 km) with winds derived from the DC-8 INS based on five flight segments. Mean biases in wind speed and direction between lidar and INS winds are 0.10 m s^{-1} and −1.4°, respectively, with standard deviations of 0.64 m s^{-1} and 2.4°, respectively. Similar agreement has been found for subsequent missions.

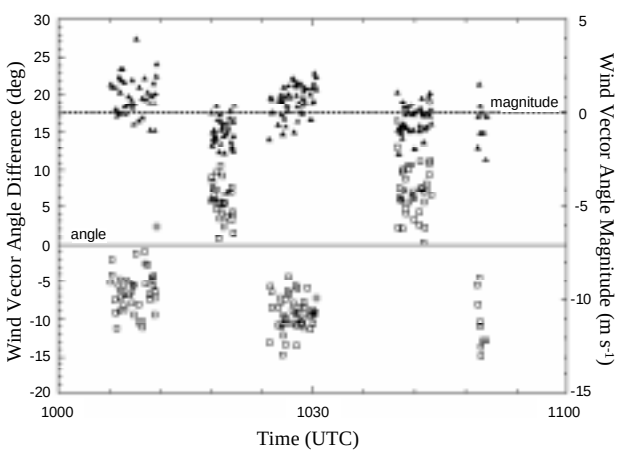

FIG. 2. Comparisons of wind speed and direction measured with MACAWS (0° elevation, minimum range ~1.2 km) and NASA DC-8 inertial navigation system on 31 May 1996 during 1006–1051 UTC at 2.13-km above mean sea level (MSL) altitude over San Joaquin Valley, California.

b. Quasi-vertical cross section

On 7 June 1996 during 1630–1813 UTC, the DC-8 flew in a series of parallel tracks in the vicinity of Napa Valley, California. During this time flight-level conditions were dominated by weak southwesterly flow due to a ridge over Utah–Arizona and by a low pressure area to the west of British Columbia, Canada. Surface conditions were influenced by a weak inverted trough extending through southern California and a stationary front located along the California–Oregon border. Figure 3 illustrates cross sections of LOS velocity and corresponding absolute aerosol backscatter observed while flying from southeast to northwest. These profiles, taken at a downward angle of 30° from horizontal, were thus pointing to the southwest and therefore measure the component of the wind in that direction. As many as seven aerosol layers are evident, most of which varied in altitude and thickness. The atmosphere below the aircraft appeared optically clear to the unaided eye. Interlayer regions are characterized by weaker scattering and marginal velocity estimates, but scattering from the clean layer between 5.0 and 6.5 km varied considerably across the swath. A distinct shear layer is evident at 3.0 km and appears to be more pronounced near the end of the run. In general, the LOS velocity distribution (southwesterly component at low level and a northeasterly component in the midtroposphere) is consistent with the surface and upper-air flow patterns.

c. Flow interaction with coastal topography

Surface winds off the California coast are northwesterly to northerly in summer, resulting from flow around the east side of the subtropical high pressure system over the Pacific Ocean. This high is accompanied by subsidence and a strong marine inversion usually a few hundred meters deep. The coastal mountain range topography interacts with the northerly flow in this marine-inversion layer to produce a variety of interesting flow phenomena. For example, when this flow passes one of the many capes and points that jut into the winds along the California coast, structures referred to as "hydraulic expansion fans" have been found (Winant et al. 1988). Such features are marked by strong variation along the vertical and cross-shore directions.

To study this variability the aircraft flew sets of parallel line segments just offshore past Point Arena on 30 June 1996 during 1950–2110 UTC at an altitude of 0.49 km. Figure 4 shows the wind distribution calculated within three scan planes; winds at two higher-elevation scan planes (not shown) were mea-

sured as well and are similar to the distribution observed at the highest angle shown in the figure. Figure 4 also serves to illustrate the wind vector displays that are available in real time. The data from all five elevation angles were reanalyzed along constant-height levels, as shown in Fig. 5. Evident is the northerly flow in the marine layer, the strong variability in the cross-shore direction within the marine layer, especially at 150 m above mean sea level (MSL), and the structural changes in the vertical. The pseudo-dual-Doppler process of calculating 2D wind velocities requires that the transformation of the original range-gated data to Cartesian grid points be executed for the fore and aft scans separately. In this case, grid spacing in the east–west and north–south directions was 300 m and 25 m in the vertical. The National Center for Atmospheric Research's software package "Custom Editing and Display of Reduced Information in Cartesian space" (Mohr and Miller 1983) was used to determine the 2D wind velocities using the two-equation solution.

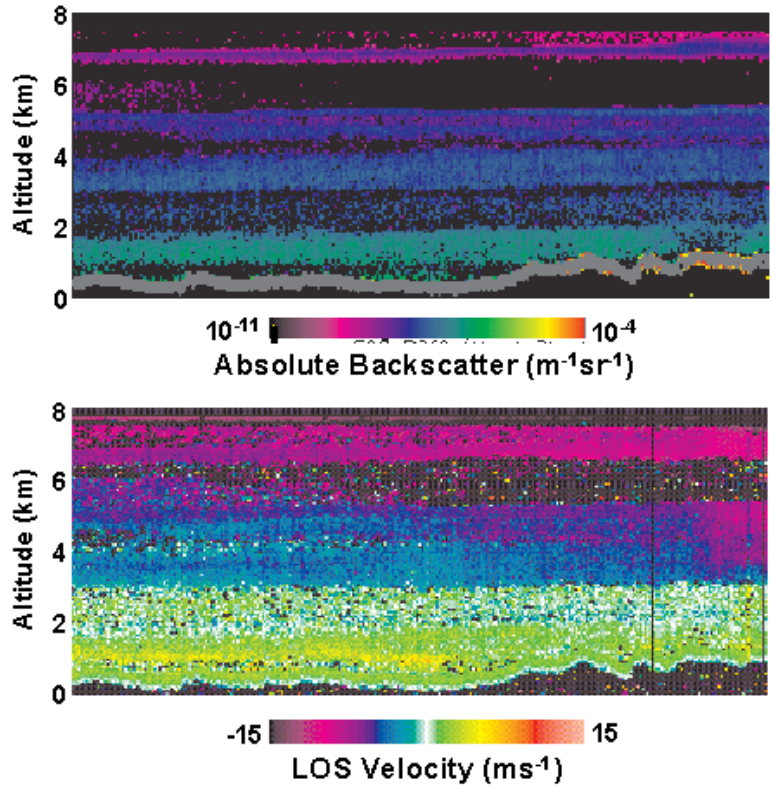

FIG. 3. Quasi-vertical cross section of aerosol backscatter coefficient (top) and line-of-sight velocity (bottom) measured on 7 June 1996 during 1715:22–1720:06 UTC with lidar beam elevation angle of –30°. Aircraft traversed a horizontal distance of ~62 km at 8.0-km MSL altitude. As many as seven scattering layers are evident, which are highly correlated with LOS velocity distribution. Lidar beam intersected land surface (indicated in gray), including western slopes of Mayacmas Mountains north of Santa Rosa, California, apparent on right-hand side. Surface reflectivities (which on average were 0.006 sr^{-1}) were computed by multiplying the absolute backscatter by the range gate width (150 m) and correcting for backscatter from a nonaerosol medium (Jarzembski et al. (1996). Ambiguity in location of these surface returns is due to laser pulse tail. Such datasets are invaluable for atmospheric research as well as to simulate aspects of the performance of prospective satellite Doppler lidar wind sounders.

5. Future research objectives

Growing demands for understanding subsynoptic-scale processes have arisen from 1) an increasing emphasis on the use of numerical models to analyze and predict subsynoptic-scale processes, and 2) the need to develop and refine parameterization schemes in numerical models used to describe the hydrological cycle and other processes influencing climatic and global change. The increased emphasis on the role of these scales, and associated scale interactions, is further underscored by research objectives of several existing or planned interagency programs, which may include enhanced observations against a background of routine measurement and research activities employing operational sensors. With spatial resolution of order 1 km, a Joule-class laser transmitter for extended propagation in optically clear air, and the range and duration afforded by a large, multiengine aircraft, MACAWS can provide unique measurements of a variety of subsynoptic-scale processes and features that are described below. The research potential of MACAWS for mesoscale studies is apparent when considering the measurement capabilities of several ground-based measurement systems under implementation. These systems, which are key components of operational meteorological and interagency research programs, include the wind profiler network (Weber et al. 1990), automated surface observing system (NOAA 1992), and National Weather Service NEXRAD (Leone et al. 1989). The wind profilers and surface observing network may be widely spaced relative to atmospheric scales of interest or else these scales may be beyond the measurement capability; some examples are given below.

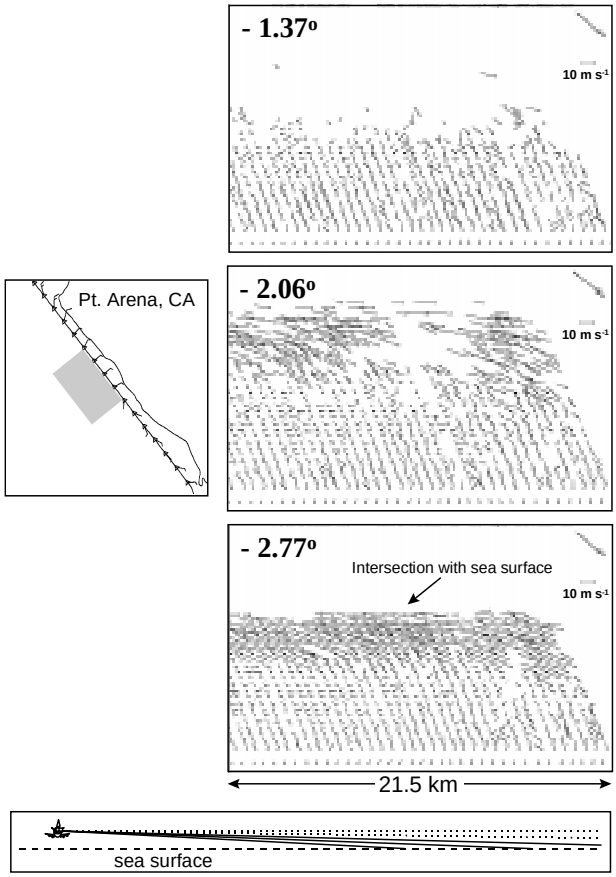

FIG. 4. Example of full-resolution wind field measurements at multiple elevation angles obtained near Point Arena, California, on 30 June 1996, 1711:34–1715:00 UTC, at ~0.49 km height MSL. Panel on left shows portion of NASA DC-8 flight track with wind velocities (kt) estimated from DC-8 inertial navigation system (INS, plotted every 1 min); this information is also displayed in real time. Shaded box indicates location of multilevel lidar wind fields shown on right-hand side. Wind fields were measured at five elevation angles, three of which are shown varying from −1.37° (top right panel, m s^{-1}) to −2.77° scan angle (bottom right); vector wind displays are representative of real-time data reduction and display capabilities. Bottom row of vectors in each panel represents aircraft INS wind estimates. Diagram at bottom depicts vertical distribution of scan planes to scale.

During 1998 and beyond, it is anticipated that MACAWS will periodically conduct research flights both independently and within the context of research programs having a field observation component. Examples of the latter include the Global Energy and Water Cycle Experiment (GEWEX) Continental-Scale International Program (GCIP) (World Climate Research Program 1992; International GEWEX Project Office 1995), the U.S. Weather Research Program (Emanuel et al. 1995; Rotunno et al. 1996), as well as other, smaller-scale interagency programs. A key goal of GCIP is the development and improvement of parameterization schemes for subgrid-scale processes within regional- and global-scale models. Measurements will be required at scales as small as 1 km, placing heavy demands on the accuracy and resolution capabilities of, among other sensors, the core observing systems identified above. The measurement capabilities of MACAWS would allow detailed measurements of, for example, the subgrid-scale momentum field, which would complement ground-based and satellite remote sensing systems. The endurance of the DC-8 permits monitoring of processes that evolve on a timescale of a few hours but that may "drift" through ground-based observing grids during evolution. MACAWS would also be well suited to studies over complex terrain, which may compromise the siting or performance of ground-based observing systems.

The remainder of this section highlights research objectives that will be addressed in 1998 and beyond, by the MACAWS team and in cooperation with interested external investigators, through independent studies or as part of multi-instrument, multiagency field programs.

a. Low-level winds and convergence in the Tropics

A number of explanations and corresponding models have been advanced to explain tropical precipitation and latent heat release, and their variation, relative to sea surface temperature. These studies challenge previous assumptions that latent heat release in deep convection strongly influences low-level convergence and that the resulting low-level moisture convergence is proportional to the amount of cumulus convection and precipitation. For example, one set of model results indicated that SST gradients produce gradients in pressure, in turn producing low-level moisture convergence, which ultimately determines the distribution of deep convection and precipitation (Lindzen and Nigam 1987). Measurement of PBL height and wind distribution with MACAWS could allow improvements to the model parameterizations. PBL height measurements would provide a check of parameterizations schemes, from which interior quantities such as temperature and moisture can be inferred.

b. Low-level jet

When the free atmosphere is decoupled from the surface at night, significant ageostrophic flow can result that is manifested by the production of a low-level jet. Previous studies of this jet have relied heavily on numerical modeling and in situ measurements by balloon soundings. While the U.S. wind profiler network

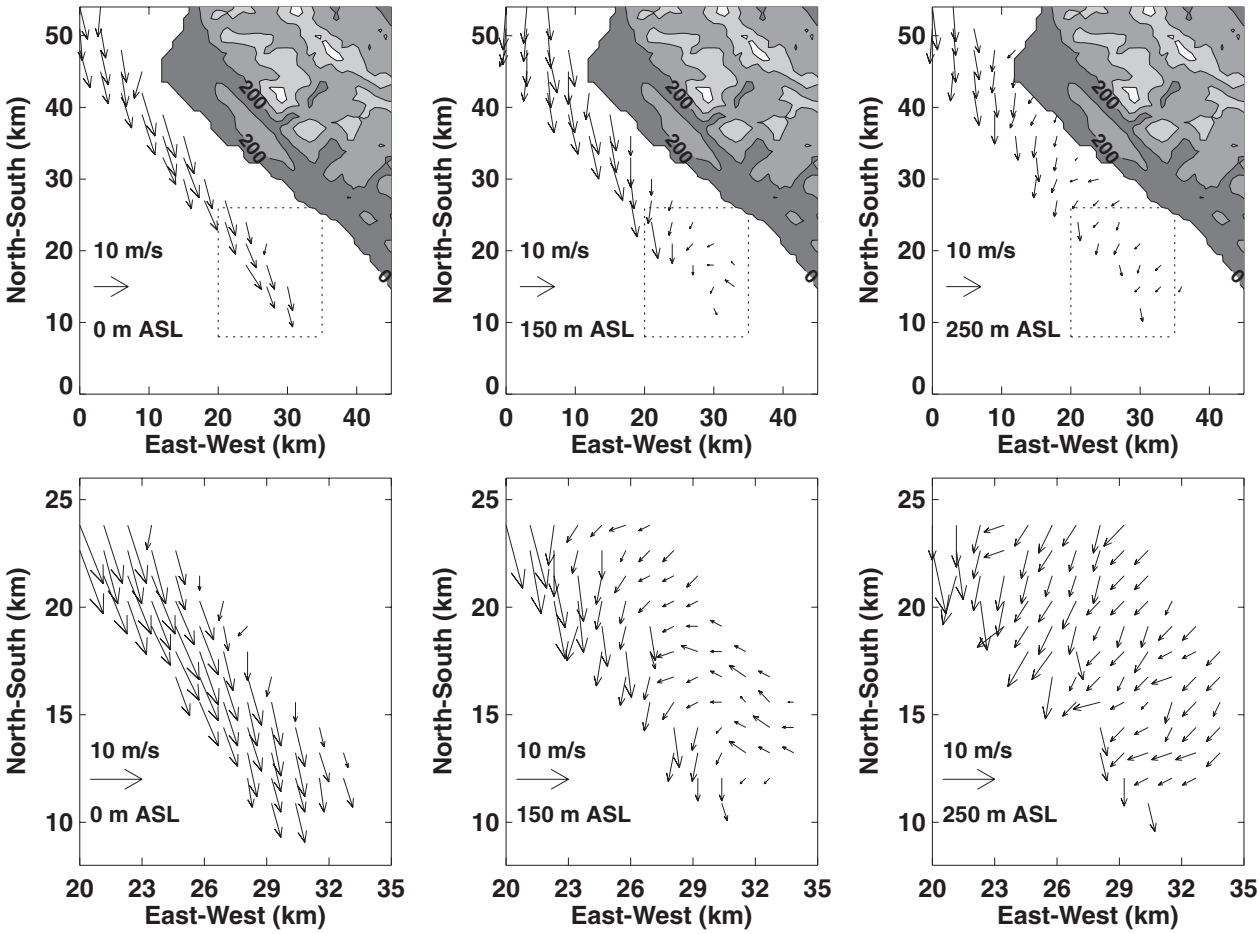

FIG. 5. Vector plots of winds based on measurements included in Fig. 4 as well as wind fields measured at two higher elevation angles (not shown). Terrain contours are in 200-m increments. Upper plots show three horizontal slices through a Cartesian grid volume at different heights ASL. Bottom plots are enlargements of the area marked by the dotted boxes above.

can be an important source of synoptic-scale measurements of this phenomenon, the lowest measurement level for these profilers may be above many low-level jets, and the vertical resolution may be rather coarse. Ground-based Doppler radars have been used successfully to measure mean and turbulent momentum quantities when the scatterers are plentiful, presumably dust, seeds, and insects (Frisch et al. 1992). The structure of the nocturnal low-level jet and the realism of the processes in numerical models that lead to its formation, however, have still not been well established. MACAWS provides a unique opportunity to probe the evolving jet with fine spatial resolution, particularly over regions that are inadequately covered by conventional sensors or where nonaerosol scatterers or complex terrain could induce biases in ground-based radar measurements (Rothermel et al. 1985). The capability of MACAWS to cover regions of ~100 km or more in less than an hour with finescale volumetric coverage make it ideal for investigating cross-jet variability, including maxima and minima in the speed of the jet, and variations in the vertical structure and vorticity.

c. Organized large eddies

Coherent structures in the PBL, sometimes referred to as organized large eddies (OLE), can affect the accuracy of PBL flux parameterizations (Foster and Brown 1991). Parameterizations based on traditional methods of boundary layer analysis utilize scattered and limited data, mostly collected over land. These parameterizations may be inaccurate (e.g., Blanc 1985) and inadequate for general circulation model studies of the climate (Randall et al. 1992). Examples of OLEs include quasi-steady 2D and 3D circulations that are often manifested, respectively, as roll vortices (Etling and Brown 1993) and mesoscale cellular convection (MCC) (Hubert 1966). Little

is known of the 3D kinematic and thermodynamic properties of individual MCC cells. Previous in situ measurements have been made in the PBL with instrumented buoys (Burt and Agee 1977) and conventional gust probes mounted on slow-flying aircraft (Rothermel and Agee 1980). Remote measurements of backscatter distribution associated with convective structures have been obtained with airborne backscatter lidar (Melfi et al. 1985). The spatial resolution, coverage, and mobility of MACAWS are ideally suited for mapping the structure of this ubiquitous marine boundary layer convective phenomenon. Preliminary measurements of a weak MCC event were obtained in and above the marine boundary layer over the northern Pacific Ocean during the 1995 MACAWS flights (not shown).

d. Tropical cyclone dynamics

New measurements are needed at multiple levels in and around the tropical cyclone. Airborne radar measurements have suggested that circulation changes may reflect intensity changes occurring above 7-km altitude, that is, rapid deepening. Since thick cirrus or heavy precipitation within the central dense overcast (CDO) may attenuate infrared laser radiation, lidar data could augment radar data in higher-altitude regions of thinner cirrus or cloud-free conditions. New measurements are needed of the flow at all levels in order to improve mass budget calculations, describe eyewall substructures, and improve understanding of eye thermodynamics. Current measurement strategies based on radar require that the eye be seeded with chaff to obtain sufficient reflectivities for Doppler observations (H. Willoughby 1995, personal communication). Additional observations are needed of tropical cyclone PBL processes, including better characterization of confluence and decelerating flow into the cyclone, and PBL entrainment. Airborne Doppler lidar cannot only measure the wind distribution in and above the PBL, but also precisely determine the PBL depth.

Recent results from a tropical cyclone prediction model developed at The Florida State University (FSU) have shown that the large-scale instabilities that arise from horizontal and vertical shear of the horizontal wind and cumulus convection are inadequate to describe the behavior of hurricanes. The modeling approach has met with success using an ensemble forecast strategy based on an operational analysis as a first guess and a physical initialization to assimilate rain rates derived from satellite observations (Krishnamurti et al. 1998a; Krishnamurti et al. 1998b; Zhang and Krishnamurti 1997). Optimal perturbations with the fastest-growing modes are then determined by a technique that employs perturbations based on empirical orthogonal functions. As a result, it should be possible to design an adaptive observational strategy that uses the findings of the ensemble-based initial states (T. N. Krishnamurti 1997, personal communication). MACAWS affords an opportunity to test the impact of Doppler lidar winds on hurricane forecasts, subject to flight conditions. During the MACAWS test flights in 1995, Doppler lidar velocity measurements were obtained within Hurricane Juliette (eastern Pacific Ocean) on 21 September 1995. Although a malfunction in the receiver—subsequently corrected—prevented full two-dimensional wind measurements, coverage of LOS winds in the CDO was observed to be 15 km or more.

Decaying landfallen tropical cyclones (TC) are known to produce tornadoes. Unprecedented NEXRAD observations of a landfalling TC of only tropical storm strength indicated the presence of persistent mesocyclones, several of which were observed to produce a series of tornadoes over South Carolina (Cammarata et al. 1996). An important issue is when the conditions for tornadogenesis arise relative to landfall. MACAWS could be used to probe rainbands within the forward quadrants of the tropical cyclone, in regions free of precipitation and with minimal clouds such as the boundary layer, in order to map out inflow patterns that may indicate mesocyclone signatures, prior and subsequent to cyclone landfall.

e. Stratosphere–troposphere exchange

MACAWS affords a unique opportunity to study the spatial and temporal scales of stratosphere–troposphere (ST) exchange by mapping flow patterns and aerosol distribution near the midlatitude tropopause. In periods when volcanic aerosol exists in the lower stratosphere and when sedimentation is not a major loss mechanism, the lower-stratospheric aerosols are useful as tracers of mass exchange. This has been depicted in a tropopause fold situation using an airborne backscatter lidar (Browell et al. 1987). Global studies of ST mass exchange clearly show zonal asymmetry and the significant influence of regional variability. When obtained near large-scale cyclonic flow patterns, MACAWS data can provide wind-vector maps of unprecedented resolution. These data should provide evidence of mixing processes associated with shear and moderate- to large-scale eddies.

f. Convective dynamics

Convection often forms initially at the boundaries between two air masses; these boundaries can range from local- to regional-scale features. Understanding and forecasting these events requires clear-air measurements of the preconvective environment near the boundaries, which are often situated in locations far removed from well-equipped, fixed observing sites. MACAWS is thus well suited to documenting these incipient circulations, such as lake-, topography-, and irrigation-induced boundary layer circulations possibly influencing deep convection (e.g., Pielke and Zeng 1989), interacting convective outflows, dryline dynamics, and mature/tornadic thunderstorms.

The dryline of the western Great Plains is an especially important boundary for severe weather production. Oriented roughly north–south, it moves east and west diurnally, and its overall location changes from week to week, emphasizing the advantage of mobile measurement systems. Variations in convergence and vorticity along its length generate hot spots for convective initiation and development. As is the case for the other phenomena described, the mobility, speed of coverage, and fine resolution of MACAWS make it an ideal platform for revealing the prestorm kinematics of the dryline. Knowledge of the evolving structure is necessary to further our understanding of processes leading to severe storm genesis and to enhance our ability to forecast severe weather with greater lead times.

g. Coastal atmospheric processes

Research into coastal processes is hampered by a lack of detailed observations. Interaction of marine boundary layer flows with coastal topography may strongly influence coastal meteorological conditions. An example has been illustrated in Figs. 4 and 5. Another example is the "southerly surge" phenomenon that can affect the meteorology of the southern California coast, in extreme cases affecting flight operations at the Los Angeles International Airport (Dorman 1985; Emanuel et al. 1995; Bond et al. 1996). Data from a weak southerly surge case were obtained during the 1996 flights and are currently being analyzed. The strengths of the MACAWS platform in investigating coastline meteorological systems make it ideal for probing the structure of these surges, and they are expected to be an important target for future research flights.

h. Comparison with scatterometer

The MACAWS team had intended to conduct calibration/validation flights against the NASA Scatterometer launched in August 1996 (Naderi et al. 1991); unfortunately, the Advanced Earth Observing Satellite spacecraft failed in June 1997 before any correlative measurements could be made. This activity will therefore focus on the NASA QuikSCAT and Sea Winds scatterometers, currently scheduled for launch in 1998 and 2000, respectively. In the meantime we plan to conduct correlative exercises with the European Remote Sensing satellite *ERS-2* scatterometer. The primary objective of the comparisons is to provide vertical profiles of horizontal wind vector within and above the marine boundary layer over regions coincident in time and spatial location with scatterometer tracks. Measurements will be obtained with horizontal resolution that is significantly finer than the fundamental resolution cell of the scatterometer. Ultimately these data will be of use in the validation and refinement of scatterometer wind vector retrieval algorithms, as well as for studies of flux parameterization schemes needed in regional and global modeling.

i. Assessment of SDWL concept

The concept of direct measurement of global tropospheric winds from space with Doppler lidar has been studied for some time (NASA 1982; Huffaker et al. 1984; Kavaya et al. 1994; Baker et al. 1995). Such measurements would fundamentally improve our understanding of global and climate change, as well as global- and regional-scale hydrological cycles (Baker et al. 1995). In the absence of a heritage of satellite Doppler lidar wind measurements, performance simulations with measured—rather than simulated—data are highly desirable to reduce uncertainties in lidar simulation models and to begin to develop the necessary interpretive skills. MACAWS can simulate several aspects of SDWL, including such issues as velocity retrievals at marginal signal levels; impact of spatial wind variability; effect of aerosol vertical gradients, particularly for near-surface wind measurements; angular dependence of sea surface returns; and, in the absence of opaque clouds, correction of velocity biases using land and ocean surface returns. Clouds will constitute a frequent scattering target for SDWL, perhaps a majority of the time. MACAWS can be used to assess velocity distribution in and around clouds, cloud porosity, cloud-free line of sight, cloud dimensions (height and possibly thickness), and optical properties (optical depth, extinction, and speckle statistics). A number of sampling strategies may also be simulated.

j. Angular dependence of sea surface scattering

The primary surface scattering target for a satellite Doppler wind lidar will be the sea surface. More-detailed measurements are necessary to better define the relationship between sea surface wind and lidar directional retroreflectance. MACAWS can be used to investigate this relationship over a larger range of nadir angles compared to measurements from the Lidar In-Space Technology Experiment (Menzies and Tratt 1996). Moreover, MACAWS employs a wavelength that does not penetrate the surface and therefore is not influenced by subsurface volume scattering. Data are valuable for both calm waters, when contributions from capillary facets are expected to dominate, and from surfaces containing significant whitecaps (foam). The spectral dependence of the foam reflectance is not well known beyond about 2 μm. To study these issues, MACAWS will employ a series of nested circular flight tracks at roll angles that will result in a nadir angle range of ~20°–70°.

6. Conclusions

In 1992 the MACAWS team set out to develop what has become perhaps the most powerful and sophisticated airborne coherent Doppler lidar system in the scientific history of atmospheric remote sensing. We have successfully achieved that goal and can now concentrate our attention on the many scientific applications of which the instrument is capable. This measurement platform fulfills decades-old dreams of those who study weather systems, by providing a 3D volume of the horizontal wind field and thus revealing the 3D kinematic structure of those systems. MACAWS is especially suited to probing flows that accompany long, linear structures, such as fronts, drylines, waves, flows near coast and mountain ranges, and determining their along-feature variability in structure; to describing the cross-feature variability of more extensive systems, such as the low-level jet; and to measuring the radial or azimuthal structural variation of atmospheric vortices such as tropical cyclones and hurricanes. One can easily envision a host of other applications.

Our experience has demonstrated that the technology necessary for the reliable operation of high-power, frequency-stable CO_2 lidar is mature and presents no technological risks. Moreover, use of a large, high-energy CO_2 laser poses no special integration problems.

Although MACAWS performance in the PBL is unique, we have identified desirable modifications that will improve measurement accuracy, resolution, and coverage. The first involves redesign of the optical table, power supply, and support structure to reduce the overall volume and mass. Preliminary estimates suggest that volume and mass can be reduced in an economic manner by nearly half. Anticipated benefits include reduced integration time, more stable operation in turbulence, and better compatibility with smaller aircraft such as a Lockheed C-130 or P3. A second desired modification is replacement of the IMU with an integrated GPS–INS package. This change would effectively eliminate, in real time, velocity errors caused by the Schuler resonance, thereby reducing the level of complexity of the postflight data processing. Other desired modifications include operation of the transmitter laser on a wavelength that is less susceptible to absorption by water vapor, for example, 11.15 μm; improvements to the electro-optical circuits in the transmitter to maintain laser frequencies with greater accuracy; replacement of the germanium wedges with diffractive optical elements to permit more rapid beam pointing; and expansion of the cooling capacity for the transmitter laser to improve temperature stability, hence performance, during ground-based tests and flights in the PBL during summer.

Finally, the MACAWS program has underscored the practical benefits of cooperation among governmental agencies during a time of shrinking research budgets. By sharing existing hardware, software, and expertise, by minimizing additional hardware development, and by identifying mutually compatible research interests, we have saved literally millions of dollars while succeeding in the development and application of a world-class airborne coherent Doppler lidar system.

Acknowledgments. We gratefully acknowledge the assistance of the following during the various stages of MACAWS development, operation, and data analysis: D. M. Chambers, Micro Craft, Inc.; E. W. McCaul Jr. and V. Srivastava, Universities Space Research Association; M. A. Jarzembski, NASA/MSFC; P. Kromis, Computer Sciences Corp.; M. A. Shapiro, F. M. Ralph, and P. J. Nieman, NOAA/ETL; H. D. Johnson, W. A. Brewer, K. Koenig, A. Weickmann, and O. Persson, Cooperative Institute for Research in Environmental Sciences (CIRES), University of Colorado at Boulder; C. Esproles, A. Coleman, A. M. Brothers, S. H. Dermenjian, R. Helms, and J. Hendrickson (now deceased), JPL; M. S. Shumate, California Institute of Technology; Conrad Ziegler, National Severe Storms Laboratory; K. R. Knupp, University of Alabama in Huntsville; and the staff and support con-

tractors of the Medium Altitude Mission Branch, NASA/Ames Research Center. We acknowledge valuable discussions with T. N. Krishnamurti, The Florida State University, and F. R. Robertson, Earth System Science Division, NASA/MSFC. This program has been funded in part by the Atmospheric Lidar Division, Environmental Technology Laboratory, NOAA/Environmental Research Laboratories. We gratefully acknowledge Dr. Ramesh Kakar, Atmospheric Dynamics and Remote Sensing Program, Office of Earth Science, NASA Headquarters, without whose support this program would not be possible.

References

American National Standards Institute, 1993: American national standard for safe use of lasers. Document Z136.1-1993, 120 pp. [Available from American National Standards Institute, 1430 Broadway, New York, NY 10018.]

Amirault, C. T., and C. A. Dimarzio, 1985: Precision pointing using a dual-wedge scanner. *Appl. Opt.,* **24,** 1302–1308.

Baker, W. E., and Coauthors, 1995: Lidar-measured winds from space: A key component for weather and climate prediction. *Bull. Amer. Meteor. Soc.,* **76,** 869–888.

Banta, R. M., L. D. Olivier, E. T. Holloway, R. A. Kropfli, B. W. Bartram, R. E. Cupp, and M. J. Post, 1992: Smoke column observations from two forest fires using Doppler lidar and Doppler radar. *J. Appl. Meteor.*, **31,** 1328–1349.

——, ——, and D. H. Levinson, 1993: Evolution of the Monterey Bay sea-breeze layer as observed by pulsed Doppler lidar. *J. Atmos. Sci.,* **50,** 3959–3982.

——, ——, W. D. Neff, D. H. Levinson, and D. Ruffieux, 1995: Influence of canyon-induced flows on flow and dispersion over adjacent plains. *Theor. Appl. Climatol.,* **52,** 27–42.

——, and Coauthors, 1997: Nocturnal cleansing flows in a tributary valley. *Atmos. Environ.,* **31,** 2147–2162.

Batten, C. E., I. M. Miller, G. M. Wood Jr., and D. V. Willetts, Eds., 1987: Closed-cycle, frequency-stable CO_2 laser technology. NASA Conf. Publ. 2456, National Aeronautics and Space Administration, 265 pp. [Available from George C. Marshall Space Flight Center, Huntsville, AL 35812.]

Bilbro, J. W., and W. W. Vaughan, 1978: Wind field measurement in the nonprecipitous regions surrounding severe storms by an airborne pulsed Doppler lidar system. *Bull. Amer. Meteor. Soc.*, **59,** 1095–1100.

——, G. H. Fichtl, D. E. Fitzjarrald, and M. Krause, 1984: Airborne Doppler lidar wind field measurements. *Bull. Amer. Meteor. Soc.,* **65,** 348–359.

——, C. A. DiMarzio, D. E. Fitzjarrald, S. C. Johnson, and W. D. Jones, 1986: Airborne Doppler lidar measurements. *Appl. Opt.,* **25,** 3952–3960.

Blanc, T. V., 1985: Variation of bulk-derived surface flux, stability, and roughness results due to the use of different transfer coefficient schemes. *J. Phys. Oceanogr.,* **15,** 650–669.

Bluestein, H. B., R. J. Doviak, M. D. Eilts, E. W. McCaul, R. Rabin, A. Sundara-Rajan, and D. S. Zrnic, 1986: Analysis of airborne Doppler lidar, Doppler radar, and tall tower measurements of atmospheric flows in quiescent and stormy weather. NASA Contractor Rep. CR-3960, 176 pp. [Available from George C. Marshall Space Flight Center, Huntsville, AL 35812.]

Blumen, W., and J. E. Hart, 1988: Airborne Doppler lidar wind field measurements of waves in the lee of Mount Shasta. *J. Atmos. Sci.,* **45,** 1571–1583.

Bond, N. A., C. F. Mass, and J. E. Overland, 1996: Coastally trapped wind reversals along the United States west coast during the warm season. Part I: Climatology and temporal evolution. *Mon. Wea. Rev.,* **124,** 430–445.

Britting, K., 1971: *Inertial Navigation Systems Analysis.* Wiley-Interscience, 249 pp.

Browell, E. V., E. F. Danielsen, S. Ismail, G. L. Gregory, and S. M. Beck, 1987: Tropopause fold structure determined from airborne lidar and in situ measurements. *J. Geophys. Res.,* **92,** 2112–2120.

Browning, K. A., and R. Wexler, 1968: The determination of kinematic properties of a wind field using a Doppler radar. *J. Appl. Meteor.,* **7,** 105–113.

Burt, W. V., and E. M. Agee, 1977: Buoy and satellite observations of mesoscale cellular convection during AMTEX 75. *Bound.-Layer Meteor.,* **12,** 3–24.

Cammarata, M., E. W. McCaul Jr., and D. Buechler, 1996: Observations of shallow supercells during a major tornado outbreak spawned by Tropical Storm Beryl. Preprints, *18th Conf. Severe Local Storms,* San Francisco, CA, Amer. Meteor. Soc., 340–343.

Carroll, J. J., 1986: Accuracy of wind measurements using an airborne Doppler lidar. *J. Atmos. Oceanic Technol.,* **3,** 3–11.

——, 1989: Analysis of airborne Doppler lidar measurements of the extended California sea breeze. *J. Atmos. Oceanic Technol.,* **6,** 820–831.

Clark, T. L., W. D. Hall, and R. M. Banta, 1994: Two- and three-dimensional simulations of the 9 January 1989 severe Boulder windstorm: Comparison with observations. *J. Atmos. Sci.,* **51,** 2317–2343.

Cliff, W. C., J. R. Skarda, D. S. Renne, and W. F. Sandusky, 1985: Analysis of the NASA/MSFC airborne Doppler lidar results from the San Gorgonio Pass California. NASA Contractor Rep. CR-3901, 69 pp. [Available from George C. Marshall Space Flight Center, Huntsville, AL 35812.]

Dorman, C. E., 1985: Evidence of Kelvin waves in California's marine layer and related eddy generation. *Mon. Wea. Rev.,* **113,** 827–839.

Eastwood, E., 1967: *Radar Ornithology.* Methuen, 278 pp.

Eilts, M. D., R. J. Doviak, and A. Sundara-Rajan, 1984: Comparison of winds, waves, and turbulence as observed by airborne lidar, ground-based radars, and instrumented tower. *Radio Sci.,* **19,** 1511–1522.

——, A. Sundara-Rajan, and R. J. Doviak, 1985: The structure of the convective atmospheric boundary layer as revealed by lidar and Doppler radars. *Bound.-Layer Meteor.*, **31,** 109–125.

Emanuel, K., and Coauthors, 1995: Report of the first prospectus development team of the U.S. Weather Research Program to NOAA and the NSF. *Bull. Amer. Meteor. Soc.*, **76,** 1194–1208.

Emmitt, G. D., 1985: Convective storm downdraft outflows detected by NASA/MSFC's 10.6 micron pulsed Doppler lidar system. NASA Contractor Rep. CR-3898, 46 pp. [Available from George C. Marshall Space Flight Center, Huntsville, AL 35812.]

Etling, D., and R. A. Brown, 1993: Roll vortices in the planetary boundary layer: A review. *Bound.-Layer Meteor.,* **65,** 215–248.

Foster, R., and R. A. Brown, 1991: An investigation into the importance of stratification, thermal wind, non-stationarity and rolls in PBL parameterizations. *Eos, Trans. Amer. Geophys. Union,* **72** (Suppl.), 79.

Fowler, M. S., and A. H. LaGrone, 1969: Comparison of insect's flight characteristics with observed characteristics of radar dot angels. *J. Appl. Meteor.,* **8,** 122–127.

Frisch, A. S., B. W. Orr, and B. E. Martner, 1992: Doppler radar observations of the development of a boundary-layer nocturnal jet. *Mon. Wea. Rev.,* **120,** 3–16.

Hardy, K. R., and H. Ottersten, 1969: Radar investigation of convective patterns in the clear atmosphere. *J. Atmos. Sci.,* **26,** 666–672.

Howell, J. N., R. M. Hardesty, J. Rothermel, and R. T. Menzies, 1996: Overview of the first Multi-center Airborne Coherent Atmospheric Wind Sensor (MACAWS) experiment: Conversion of a ground-based lidar for airborne applications. *Proc. Soc. Photo. Instrum. Eng.,* **2833,** 116–127.

Hubert, L. F., 1966: Mesoscale cellular convection. Meteor. Satellite Lab. Rep. 37, 68 pp. [Available from U.S. Dept. Commerce, Washington, DC 20228.]

Huffaker, R. M., M. J. Post, J. T. Priestley, F. F. Hall Jr., R. A. Richter, and R. J. Keeler, 1984: Feasibility studies for a global wind measuring satellite system (WINDSAT): Analysis of simulated performance. *Appl. Opt.,* **22,** 1655–1665.

International GEWEX Project Office, 1995: Major activities plan for 1996, 1997 and outlook for 1998 for the GEWEX Continental-scale International Project (GCIP). IGPO Publication Series 16, 142 pp. [Available from International GEWEX Project Office, 1100 Wayne Ave., Suite 120, Silver Spring, MD 20910.]

Intrieri, J. M., G. L. Stephens, W. L. Eberhard, and T. Uttal, 1993: A method for determining cirrus cloud particle sizes using a lidar and radar backscatter technique. *J. Appl. Meteor.,* **32,** 1074–1082.

——, W. L. Eberhard, T. Uttal, J. A. Shaw, J. B. Snider, Y. Han, and B. W. Orr, 1995: Multiwavelength observations of a developing cloud system: The FIRE II 26 November 1991 case study. *J. Atmos. Sci.,* **52,** 4079–4093.

Jarzembski, M. A., V. Srivastava, and D. M. Chambers, 1996: Lidar calibration technique using laboratory-generated aerosols. *Appl. Opt.,* **35,** 2096–2108.

Jelalian, A. V., W. H. Keene, and C. M. Sonnenschein, 1972: Development of CO_2 laser Doppler instrumentation for detection of clear air turbulence. Final report, Raytheon Co., NAS8-24742, 154 pp. [Available from George C. Marshall Space Flight Center, Huntsville, AL 35812].

Kavaya, M. J., and R. T. Menzies, 1985: Lidar aerosol backscatter measurements: Systematic, modeling, and calibration error considerations. *Appl. Opt.,* **24,** 3444–3453.

——, G. D. Spiers, E. S. Lobl, J. Rothermel, and V. W. Keller, 1994: Direct global measurements of tropospheric winds employing a simplified coherent laser radar using fully scalable technology and technique. *Proc. Photo-opt. Instrum. Eng.,* **2214,** 237–249.

Krishnamurti, T. N., C. E. Williford, and R. C. Torres, 1998a: Tropical cyclone forecasts made with the FSU global spectral model. *Mon. Wea. Rev.,* in press.

——, B. Jha, W. Hau, and H. S. Bedi, 1998b: Numerical prediction of Hurricane Opal. *Mon. Wea. Rev.,* in press.

Lee, R. W., and K. A. Lee, 1980: A poly-pulse-pair signal processor for coherent Doppler lidar. Preprints, *Topical Meeting on Coherent Laser Radar for the Atmos.,* Aspen, CO, Opt. Soc. Amer., 1–4.

Leone, D. A., R. M. Endlich, J. Petriceks, R. T. H. Collis, and J. R. Porter, 1989: Meteorological considerations used in planning the NEXRAD network. *Bull. Amer. Meteor. Soc.,* **70,** 4–12.

Lhermitte, R. M., and D. Atlas, 1961: Precipitation motion by pulse Doppler lidar. *Proc. Ninth Weather Radar Conf.,* Boston, MA, Amer. Meteor. Soc., 218–223.

Lindzen, R. S., and S. Nigam, 1987: On the role of sea surface temperature gradients in forcing low-level winds and convergence in the tropics. *J. Atmos. Sci.,* **44,** 2418–2436.

McCaul, E. W., Jr., H. B. Bluestein, and R. J. Doviak, 1986: Airborne Doppler lidar techniques for observing severe thunderstorms. *Appl. Opt.,* **25,** 698–708.

——, ——, and ——, 1987: Airborne Doppler lidar observations of convective phenomena in Oklahoma. *J. Atmos. Oceanic Technol.,* **4,** 479–497.

Megie, G., and R. T. Menzies, 1979: Tunable single-longitudinal-mode operation of an injection-locked TEA CO_2 laser. *Appl. Phys. Lett.,* **35,** 835–838.

Melfi, S. H., J. D. Spinhirne, S. H. Chou, and S. P. Palm, 1985: Lidar observations of vertically organized convection in the planetary boundary layer over the ocean. *J. Climate Appl. Meteor.,* **24,** 806–821.

Menzies, R. T., 1986: Doppler lidar atmospheric wind sensors: A comparative performance evaluation for global measurement applications from earth orbit. *Appl. Opt.,* **25,** 2546–2553.

——, and R. M. Hardesty, 1989: Coherent Doppler lidar for measurements of wind fields. *Proc. IEEE,* **77,** 449–462.

——, and D. M. Tratt, 1994: Airborne CO_2 coherent lidar for measurements of atmospheric aerosol and cloud backscatter. *Appl. Opt.,* **33,** 5698–5711.

——, and ——, 1996: Ocean surface wind speed determination with LITE surface directional reflectance measurements. Abstract Digest, *Int. Laser Radar Conf.,* Berlin, Germany, International Coordination Group on Laser Atmos. Studies, 76.

Mohr, C. G., and L. J. Miller, 1983: CEDRIC—A software package for Cartesian space editing, synthesis, and display of radar fields under interactive control. Preprints, *21st Conf. on Radar Meteorology,* Edmonton, AB, Canada, Amer. Meteor. Soc., 569–574.

Naderi, F. M., M. H. Freilich, and D. G. Long, 1991: Spaceborne radar measurement of wind velocity over the ocean—An overview of the NSCAT scatterometer system. *Proc. IEEE,* **79,** 850–866.

NASA, 1982: Feasibility assessment: Satellite Doppler lidar wind measuring system. NASA Rep. MSFC-MOSD-146, 182 pp. [Available from George C. Marshall Space Flight Center, Huntsville, AL 35812].

——, 1987: Laser atmospheric wind sounder. Earth Observing System Instrument Panel Report Vol. IIg, NASA Rep. MSFC-MOSD-146, 55 pp. [Available from NASA, Office of Earth Science, Washington, DC 20546.]

——, 1994: DC-8 airborne laboratory experimenters handbook. 164 pp. [Available from NASA/Ames Research Center, Moffett Field, CA 94035].

NOAA, 1992: *ASOS Users Guide.* U.S. Government Printing Office, 85 pp.

Pielke, R. A., and X. Zeng, 1989: Influence on severe storm development of irrigated land. *Natl. Wea. Dig.*, **14,** 16–17.

Post, M. J., and R. E. Cupp, 1990: Optimizing a pulsed Doppler lidar. *Appl. Opt.*, **29,** 4145–4158.

Ralph, F. M., P. J. Neiman, T. L. Keller, D. H. Levinson, and L. S. Fedor, 1997: Observations, simulations, and analysis of nonstationary trapped lee waves. *J. Atmos. Sci.*, **54,** 1308–1333.

Randall, D. A., and Coauthors, 1992: Intercomparison and interpretation of surface energy fluxes in atmospheric general circulation models. *J. Geophys. Res.*, **97,** 3711–3734.

Richmond, R., and D. Jewell, 1997: U.S. Air Force ballistic winds program. Preprints, *Ninth Conf. on Coherent Laser Radar*, Linköping, Sweden, Swedish Defence Research Establishment, 304–307.

Rothermel, J., 1987: Results from 1984 airborne Doppler lidar wind measurement program: Flight 6: Analysis of line-of-sight elevation angle errors and apparent Doppler velocities. NASA Contractor Rep. CR-178994, 18 pp. [Available from George C. Marshall Space Flight Center, Huntsville, AL 35812.]

——, and E. M. Agee, 1980: Aircraft investigation of mesoscale cellular convection during AMTEX 75. *J. Atmos. Sci.*, **37,** 1027–1040.

——, C. Kessinger, and D. L. Davis, 1985: Dual-Doppler lidar measurement of winds in the JAWS experiment. *J. Atmos. Oceanic Technol.*, **2,** 138–147.

——, D. A. Bowdle, J. M. Vaughan, and M. J. Post, 1989: Evidence of a tropospheric aerosol backscatter background mode. *Appl. Opt.*, **28,** 1040–1042.

Rotunno, R., and Coauthors, 1996: Coastal meteorology and oceanography: Report of the Third Prospectus Development Team of the U.S. Weather Research Program to NOAA and NSF. *Bull. Amer. Meteor. Soc.*, **77,** 1578–1585.

Rye, B. J., and R. M. Hardesty, 1993: Discrete spectral peak estimation in incoherent backscatter heterodyne lidar. Part II. Correlogram accumulation. *IEEE Trans. Geosci. Remote Sens.*, **31,** 28–35.

——, and ——, 1994: Spectral matched filters in coherent laser radar. *J. Modern Opt.*, **41,** 2131–2144.

Targ, R., and Coauthors, 1996: Coherent lidar airborne wind sensor II: Flight test results at 2 and 10 μm. *Appl. Opt.*, **35,** 7117–7127.

Theon, J. S., W. W. Vaughan, E. V. Browell, W. D. Jones, M. P. McCormick, S. H. Melfi, R. T. Menzies, G. K. Schwemmer, and J. D. Spinhirne, 1991: NASA's program in lidar remote sensing. *Proc. Soc. Photo-opt. Instrum. Eng.*, **1492,** 2–23.

Wakimoto, R. M., W.-C. Lee, H. B. Bluestein, C.-H. Liu, and P. H. Hildebrand, 1996: ELDORA observations during VORTEX 95. *Bull. Amer. Meteor. Soc.*, **77,** 1465–1481.

Weber, B. L., R. G. Strauch, D. A. Merritt, and K. P. Moran, 1990: Preliminary evaluation of the first NOAA demonstration network wind profiler. *J. Atmos. Oceanic Technol.*, **7,** 909–918.

Werner, C., P. Flamant, F. Köpp, C. Loth, H. Herrmann, J. Wildenauer, A. Dolfi-Bouteyre, and G. Ancellet, 1989: WIND: An advanced wind infrared Doppler lidar for mesoscale meteorological studies. Phase O/A Study Report to DLR and CNRS, 242 pp. [Available from DLR Institute of Optoelectronics, P.O. Box 1116, D-82230 Wessling, Federal Republic of Germany.]

Wilson, J., R. Carbone, H. Baynton, and R. Serafin, 1980: Operational application of meteorological Doppler radar. *Bull. Amer. Meteor. Soc.*, **61,** 1154–1168.

Winant, C. D., C. E. Dorman, C. A. Friehe, and R. C. Beardsley, 1988: The marine layer off northern California: An example of supercritical channel flow. *J. Atmos. Sci.*, **45,** 3588–3605.

World Climate Research Programme, 1992: Scientific plan for the GEWEX Continental-Scale International Project (GCIP). WRCR-67 WMO/TD No. 461, 65 pp. [Available from International GEWEX Project Office, 100 Wayne Ave., Suite 120, Silver Spring, MD 20910.]

Zhang, Z., and T. N. Krishnamurti, 1997: Ensemble forecasting of hurricane tracks. *Bull. Amer. Meteor. Soc.*, **78,** 2785–2795.